Electronic Supplementary Information

Ultrafine copper nanoclusters and single sites for Fenton-like reactions with high atom utilities

Yu Yin[a,b], Wenlang Li[c], Chunli Xu[a], Lei Shi[b], Lai-Chang Zhang[b], Zhimin Ao[c], Mengxuan Liu[a], Min Lu[a], Xiaoguang Duan[d], Shaobin Wang[d,*], Shaomin Liu[e], and Hongqi Sun[b,*]

[a] School of Environmental and Chemical Engineering, Jiangsu University of Science and Technology, Zhenjiang, 212003, China

[b] School of Engineering, Edith Cowan University, 270 Joondalup Drive, Joondalup, WA 6027, Australia

[c] Guangdong Key Laboratory of Environmental Catalysis and Health Risk Control, Institute of Environmental Health and Pollution Control, School of Environmental Science and Engineering, Guangdong University of Technology, Guangzhou, 510006, China

[d] School of Chemical Engineering, The University of Adelaide, Adelaide, SA 5005, Australia

[e] WA School of Mines: Minerals, Energy and Chemical Engineering, Curtin University, WA 6102, Australia

[*] Corresponding Authors

Email: h.sun@ecu.edu.au (H. Sun); shaobin.wang@adelaide.edu.au (S. Wang)

Supporting Experimental Section

Experimental Section

Characterizations.

The copper loadings were determined by inductively coupled plasma optical emission spectrometry (ICP-OES) on an Optima 7300 DV instrument (PerkinElmer Corporation).Transmission electron microscopy (TEM) images were taken on a JEM-200CX electron microscope operated at 200 kV. Fourier transform infrared (FT-IR) spectroscopy was recorded on a PerkinElmer instrument. The thermal decomposition profiles were measured on a thermogravimetric analyzer (PerkinElmer TGA 4000) by heating samples from room temperature to 900 ^{o}C at a rate of 10 ^{o}C·min^{-1} in 20 mL·min^{-1} of an air flow.

Supporting Results and Discussion

Cu sites in UNCu-SBA are highly dispersed in the form of ultra-small nanoclusters combining with single atoms. However, copper aggregated into particles in APCu-SBA. The only difference between UNCu-SBA and APCu-SBA during the synthesis route was employing SBA-15 with or without P123 as the support. The proposed mechanism for the better dispersion of Cu sites in UNCu-SBA than APCu-SBA was then investigated according to the results of FT-IR and TG profiles. As shown in Figures S6A and S6C, on the spectra of P123/SBA, the stretching and bending vibrations at 2850 – 3000 and 1350 – 1500 cm^{-1} results from P123. The peaks appeared at 960 cm^{-1} are ascribed to silicon hydroxyl (Si-OH) groups. Notably, after annealing, the P123 peaks disappear entirely, and the Si-OH signals greatly decline on the spectra of SBA-15 (Figures S6B and S6D). These observations indicate that total P123 and massive Si-OH have been removed in SBA-15. That is to say, P123/SBA-15 reserves more Si-OH than SBA-15, which is regarded as the link between the host of SBA-15 and guest of Cu sites in the form of Si-O-Cu. More Si-OH are favorable to the formation of Si-O-Cu and less CuO, thus no large CuO particles.

Figure S7 describes the TG and DTG curves of P123/SBA-15, UNCu-SBA and APCu-SBA. A sharp weight loss on P123/SBA-15 centering at 184 ^{o}C is attributed to the decomposition of P123. This temperature is found to be lower than the pure P123 (210 ^{o}C), which should be as a result of the catalysis of silica walls to P123. It should be pointed out that the temperature for P123 decomposition in UNCu-SBA greatly improves up to about 280 ^{o}C. This gives evidence for the incorporation of $Cu(NO_3)_2$ into the confined space between P123 and silica walls, therefore P123 is separated from the silica walls. In addition, $Cu(NO_3)_2$ decomposition takes place at about 200 ^{o}C, prior to the destroy of P123. Consequently, the aggregation of copper species are restricted because of the confined space in P123/SBA-15. In summary, the synergistic effect of abundant Si-OH and confined space in P123/SBA-15 lead to the formation of ultra-small CuO nanoclusters and single atom Cu. Less Si-OH and loss of confined space give rise to the CuO particle aggregation.

Supporting Figures and Tables

Table S1. Textural properties of SBA-15, UNCu-SBA and APCu-SBA samples.

Sample	Cu loading [a] (mmol·g^{-1}(SBA-15))	S_{BET} (m^2·g^{-1})	V_p (cm^3·g^{-1})	D_p (nm)		a_0 [b] (nm)
				adsorption	desorption	
SBA-15	−	796	1.023	8.2	6.3	10.8
0.125UNCu-SBA	0.126	783	0.992	9.1	6.9	11.5
0.25UNCu-SBA	0.25	776	0.993	8.7	6.9	11.5
0.5UNCu-SBA	0.51	684	0.881	8.3	6.4	11.5
1.0UNCu-SBA	1.03	657	0.855	8.2	6.4	11.5
0.125APCu-SBA	0.125	661	0.845	8.2	6.3	10.8
0.25APCu-SBA	0.24	624	0.797	7.7	6.3	10.8
0.5APCu-SBA	0.52	605	0.789	7.7	6.3	10.8
1.0APCu-SBA	1.00	596	0.766	7.7	6.3	10.8

[a] Determined by ICP-OES. [b] Unit cell constant calculated according to $a_0 = 2 \times 3^{-1/2} \times d_{100}$.

Table S2. Structural parameters extracted from the Fe K-edge EXAFS fitting. (S_0^2 = 0.87)

Sample	Scattering pair	CN	R (nm)	σ^2 (10^{-3}Å^2)	ΔE_0 (eV)	R factor
Cu foil	Cu-Cu	12	0.254	5.1	3.78	0.002
Cu_2O	Cu-O	2	0.185	6.2	6.81	0.030
CuO	Cu-O	4	0.195	3.1	2.57	0.010
0.5UNCu-SBA	Cu-O	3.37	0.194	5.1	8.22	0.002
	Cu-(O)-Si/Cu	3.54	0.281	9.5	9.81	
	Cu-(O)-Si/Cu	2.23	0.312	7.8	6.48	
0.5APCu-SBA	Cu-O	3.89	0.195	4.0	1.21	0.006
	Cu-O	1.86	0.281	5.3	8.00	
	Cu-(O)-Cu	3.13	0.312	9.4	9.84	

S_0^2 is the amplitude reduction factor; CN is the coordination number; R is interatomic distance (the bond length between central atoms and surrounding coordination atoms); σ^2 is Debye-Waller factor (a measure of thermal and static disorder in absorber-scatterer distances); ΔE_0 is edge-energy shift (the difference between the zero kinetic energy value of the sample and that of the theoretical model). R factor is used to value the goodness of the fitting.

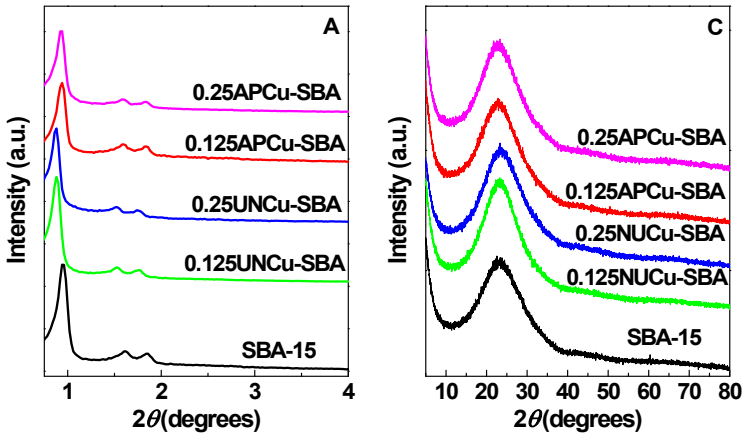

Figure S1. (A) Low-angle and (B) wide-angle XRD patterns of SBA-15, UNCu-SBA and APCu-SBA samples.

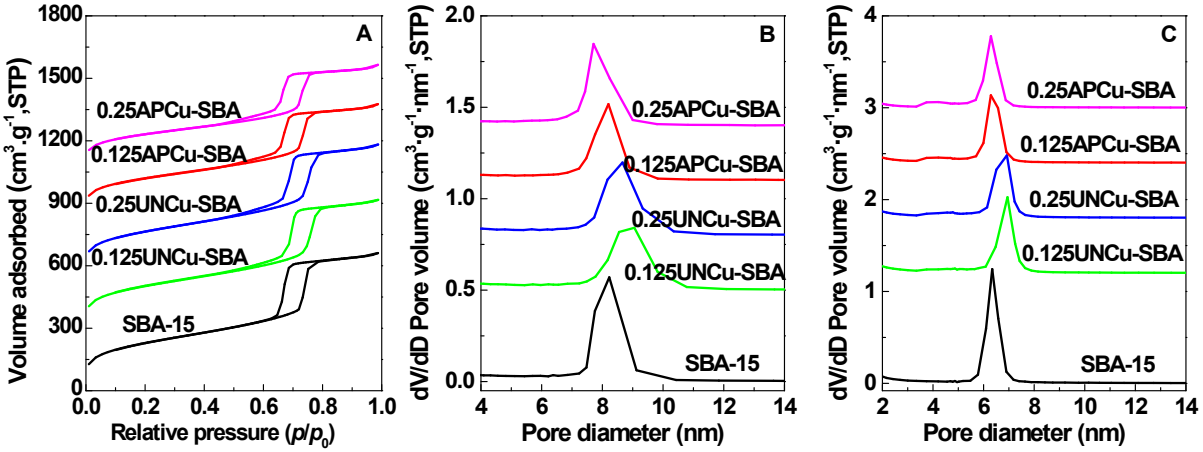

Figure S2. (A) N_2 adsorption-desorption isotherms and pore size distributions calculated by (B) adsorption and (C) desorption branches of the isotherms of SBA-15, UNCu-SBA and APCu-SBA samples. Curves are plotted offset for clarity.

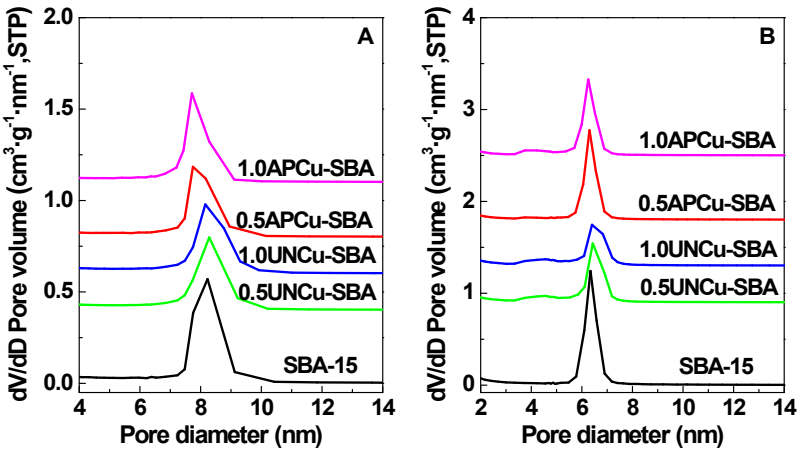

Figure S3. Pore size distributions calculated by (A) adsorption and (B) desorption branches of the isotherms of SBA-15, UNCu-SBA and APCu-SBA samples. Curves are plotted offset for clarity.

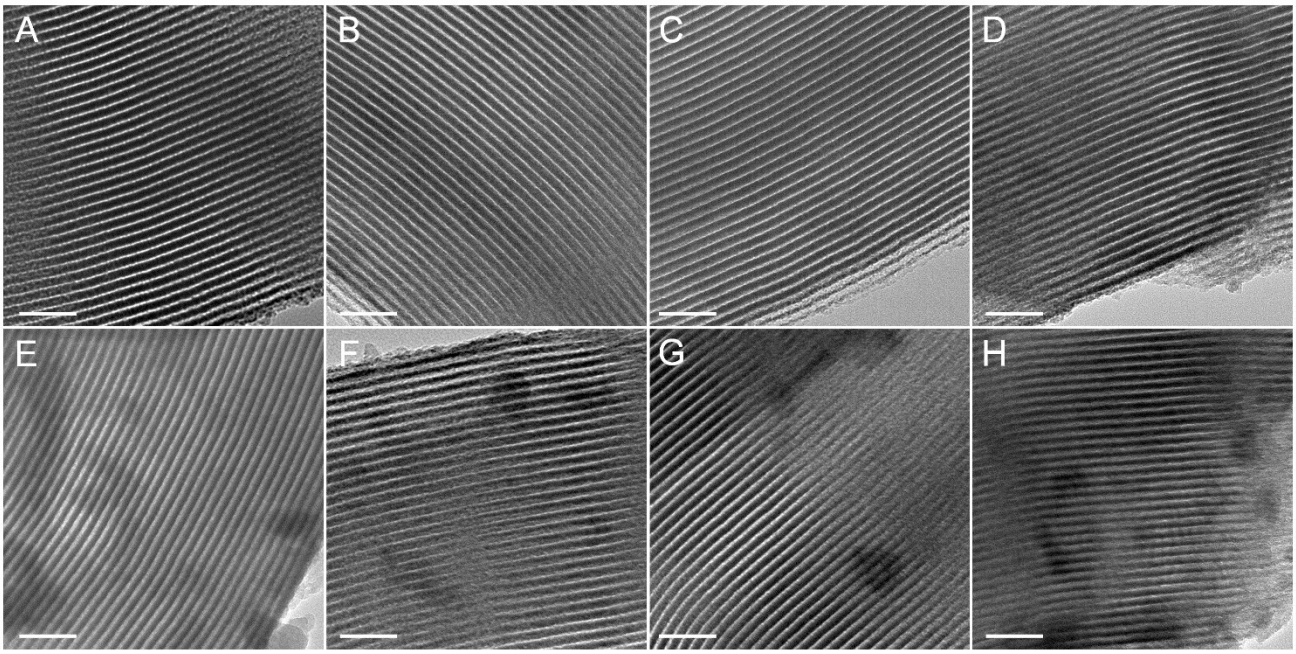

Figure S4. TEM images of (A) 0.125UNCu-SBA, (B) 0.25UNCu-SBA, (C) 0.5UNCu-SBA, (D) 1.0UNCu-SBA and (E) 0.125APCu-SBA, (F) 0.25APCu-SBA, (G) 0.5APCu-SBA, (H) 1.0APCu-SBA. Scale bars: 50 nm.

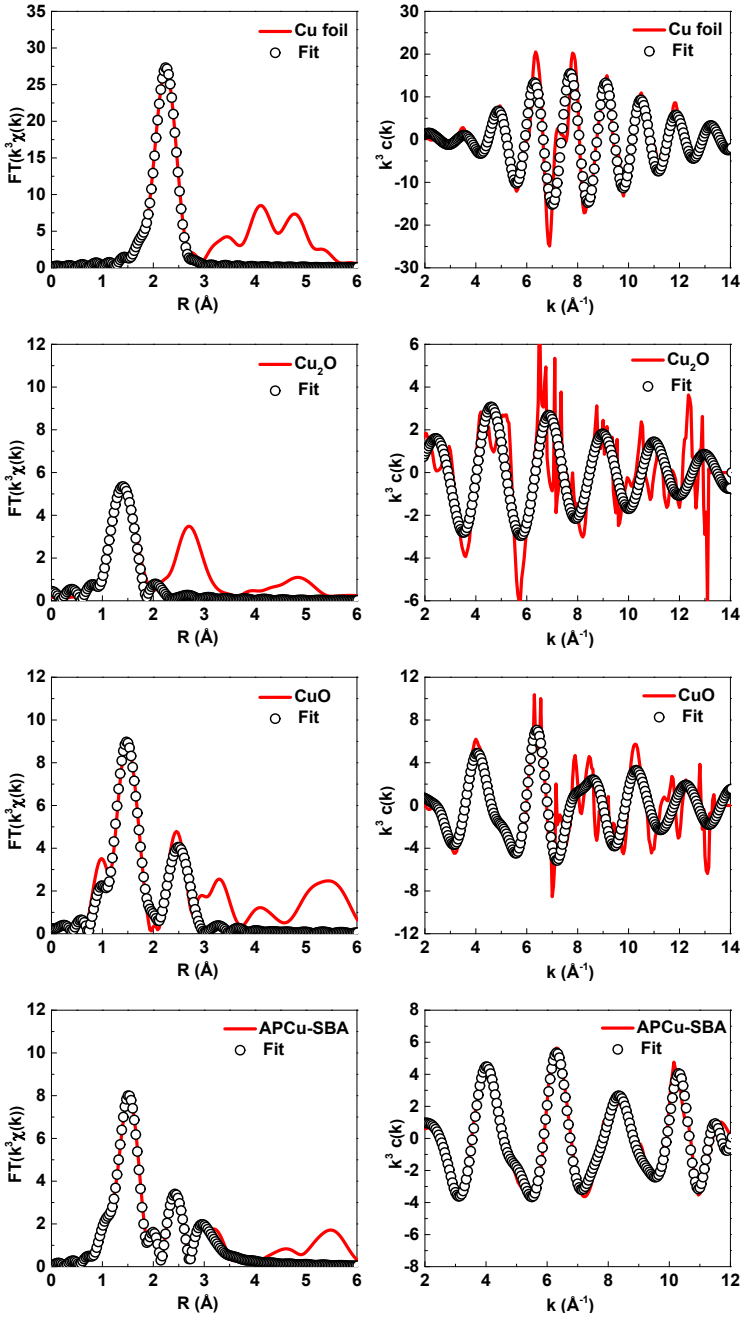

Figure S5. The EXAFS R, k space fitting curves of Cu foil, Cu_2O, CuO and APCu-SBA.

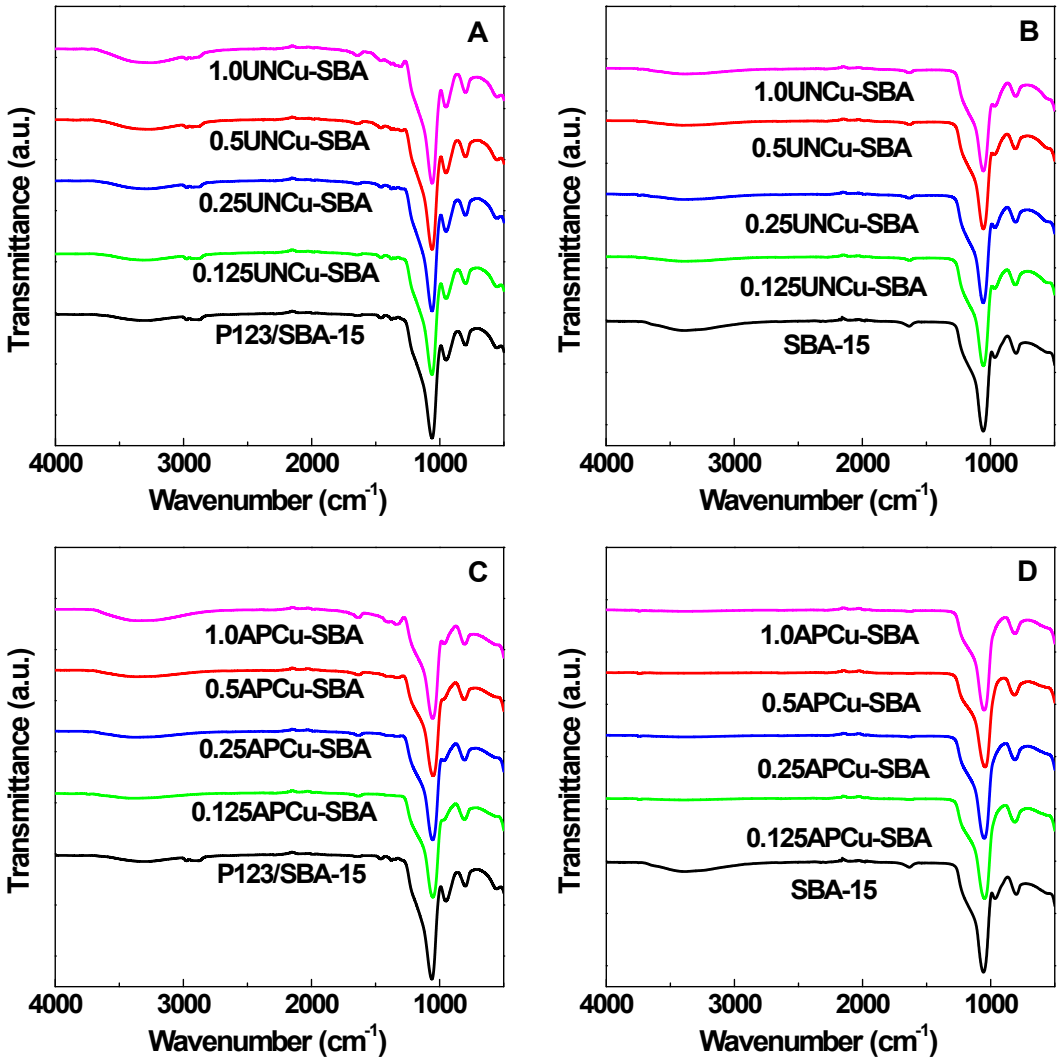

Figure S6. FT-IR spectra of SBA-15, UNCu-SBA and APCu-SBA samples. (A, C) before and (B, D) after annealing.

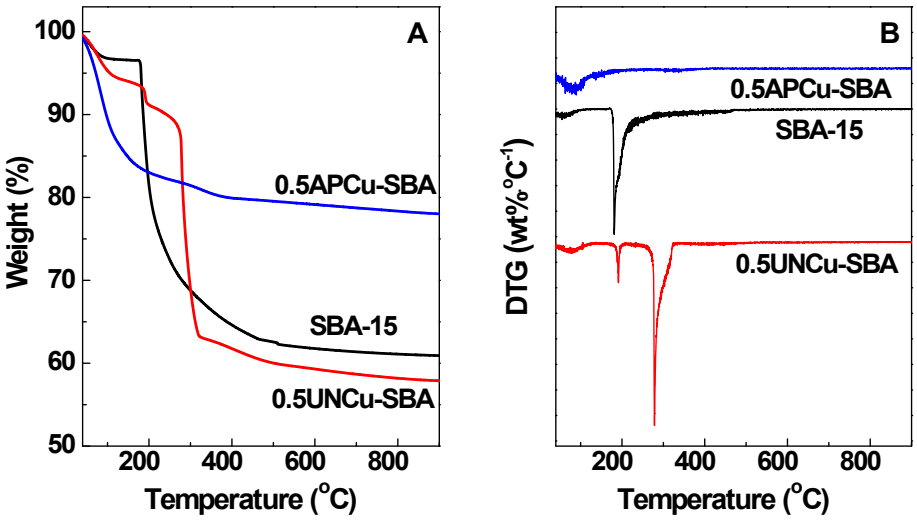

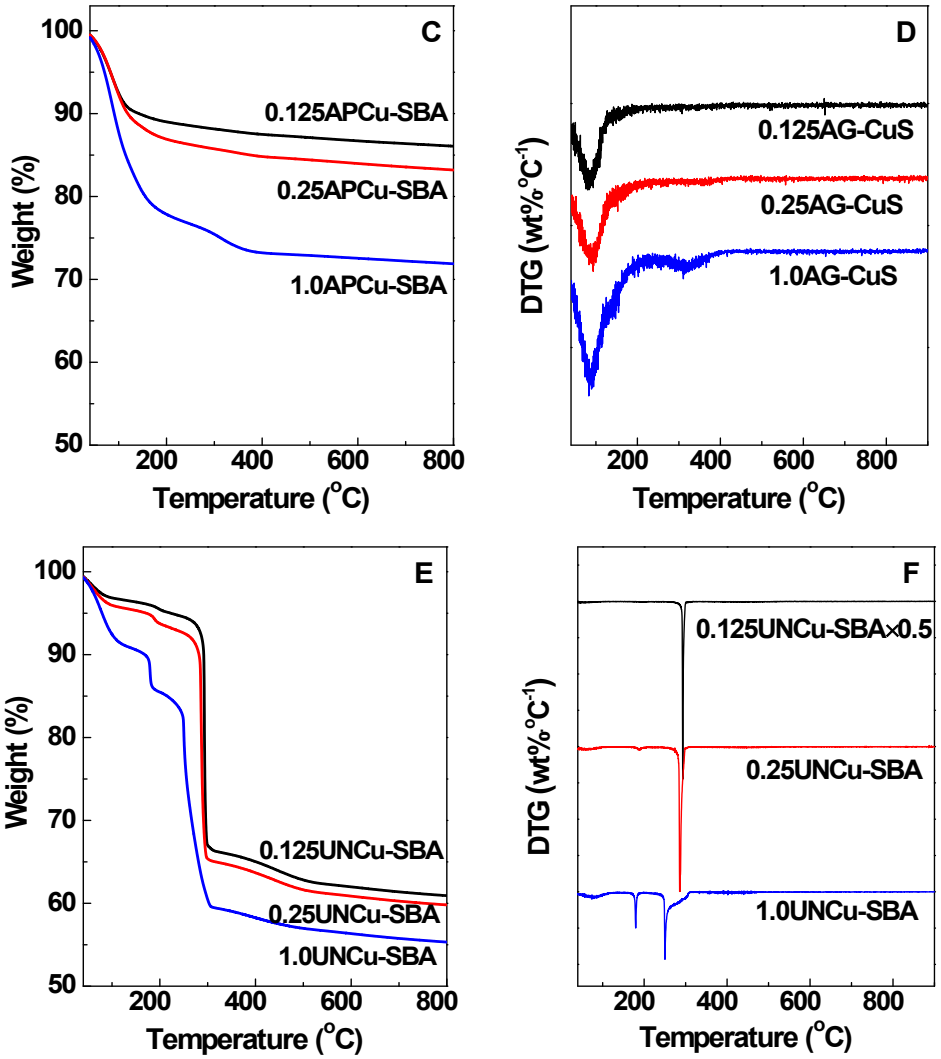

Figure S7. (A, C, E) TG and (B, D, F) DTG curves of SBA-15, UNCu-SBA and APCu-SBA samples before calcination. DTG curves are plotted offset for better clarity.

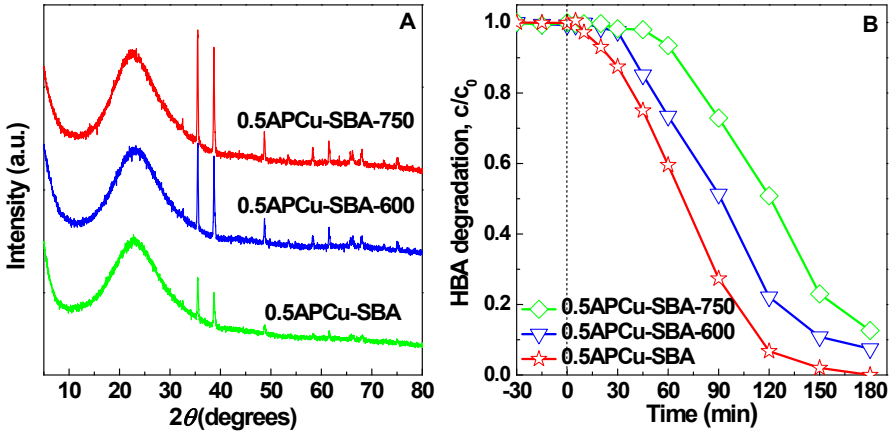

Figure S8. (A) Wide-angle XRD patterns, (B) adsorption and oxidation of HBA by H_2O_2 activation on 0.5APCu-SBA-T catalysts. ($[Catalyst]_0$ = 0.2 g·L^{-1}, $[H_2O_2]_0$ = 1000 ppm, [T] = 40 °C, and $[HBA]_0$ = 20 mg·L^{-1}).

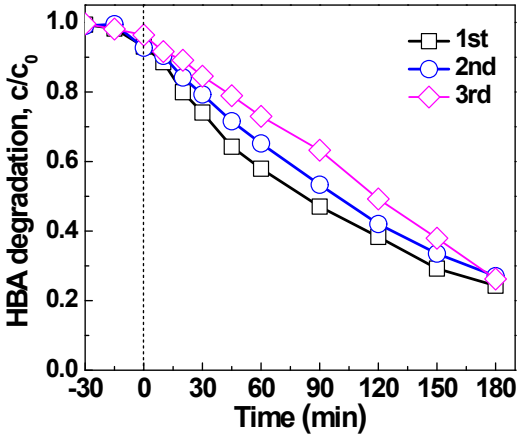

Figure S9. Cyclic adsorption and oxidation of HBA by H_2O_2 activation on 0.5UNCu-SBA catalysts. ($[Catalyst]_0$ = 0.2 g·L^{-1}, $[H_2O_2]_0$ = 1000 ppm, [T] = 40 °C, and $[HBA]_0$ = 20 mg·L^{-1}, constant pH = 7).